2890 *Biochemistry* **2010,** *49,* 2890–2896
DOI: 10.1021/bi902050p

BIOCHEMISTRY
including biophysical chemistry & molecular biology
Article

The Crystal Structure of the Human Nascent Polypeptide-Associated Complex Domain Reveals a Nucleic Acid-Binding Region on the NACA Subunit[†,‡]

Yiwei Liu, Yingxia Hu, Xu Li, Liwen Niu,* and Maikun Teng*

Hefei National Laboratory for Physical Sciences at Microscale and School of Life Sciences, University of Science and Technology of China, Hefei, Anhui 230027, China and Key Laboratory of Structural Biology, Chinese Academy of Sciences, Hefei, Anhui 230027, China

Received December 1, 2009; Revised Manuscript Received March 8, 2010

ABSTRACT: In archaea and eukaryotes, the nascent polypeptide-associated complex (NAC) is one of the cytosolic chaperones that contact the nascent polypeptide chains as they emerge from the ribosome and assist in post-translational processes. The eukaryotic NAC is a heterodimer, and its two subunits form a stable complex through a dimerizing domain called the NAC domain. In addition to acting as a protein translation chaperone, the NAC subunits also function individually in transcriptional regulation. Here we report the crystal structure of the human NAC domain, which reveals the manner of human NAC dimerization. On the basis of the structure, we identified a region in the NAC domain of the human NAC α-subunit as a new nucleic acid-binding region, which is blocked from binding nucleic acids in the heterodimeric complex by a helix region in the *β*-subunit.

A ribosome is the molecular factory where protein synthesis occurs. Newly synthesized proteins exit the ribosome as unfolded polypeptide chains that must achieve a specific three-dimensional structure to become functionally active. A large number of molecular chaperones, including the nascent polypeptide-associated complex (NAC), heat-shock proteins, prefoldin, etc., associate with the newly synthesized polypeptide chains to protect them from aggregation and degradation by cytosolic proteolytic enzymes and to help them fold properly (*1*, *2*).

In archaea and eukaryotes, NAC is one of the first cytosolic chaperones to contact the nascent polypeptide chains as they emerge from the ribosome (*3*). It is located at the nascent polypeptide exiting site of the ribosome by binding to ribosomal protein L23 (or its homologues), which is positioned near the exiting site and functions as a binding platform for cytosolic factors interacting with nascent chains (*2*, *4*). NAC interacts with unfolded polypeptide chains and is proposed to contribute to the fidelity of cotranslational processes such as folding and targeting of the nascent proteins (*3*, *5*, *6*). It also regulates translocation of protein into the endoplasmic reticulum and mitochondria (*7*−*10*). Recent studies showed that its stability and functions are regulated by ubiquitination (*11*−*13*). In addition, the individual subunits of NAC also have roles in transcriptional regulation-related processes and in cell differentiation (*14*−*22*). Despite extensive investigations, the exact function of NAC is still not fully understood.

Human NAC (hNAC) contains two subunits, α-NAC (NACA) and *β*-NAC (BTF3). Both contain a featured domain named the NAC domain that mediates dimerization of the two subunits, and the NACA subunit has an extra ubiquitin-associated (UBA) domain at the C-terminal end (Figure 1). To better understand the NAC, we elucidated the crystal structure of the NAC domain of human NAC at 2.5 Å resolution. The NAC domains of the two subunits form a compact *β*-barrel with their *β*-strands. The structure is highly similar to the NAC domain of the archaeal NAC, but with additional features (*23*). A positively charged region on NACA was shown to be covered by a helix region from BTF3. On this basis, we identified this region on NACA as a nucleic acid-binding region. These results provide possible explanations for the functional regulation of NAC and improve our understanding of the biological functions of NAC in eukaryotes.

MATERIALS AND METHODS

Plasmid Construction, Protein Expression, and Purification. Genes of NACA (GeneID 4666) and BTF3 (GeneID 689) were amplified from the human cDNA library by using a standard polymerase chain reaction (PCR) protocol. Primers used in cloning were synthesized by Sangon (Shanghai, China), and the sequences are summerized in Table S1 of the Supporting Information. The N-terminal 83-residue truncated NACA (NACAΔN) gene was then cloned into the NdeI and XhoI sites of pET22b(+) (Novagen), and the N-terminal 95-residue truncated BTF3 (BTF3ΔN) gene was cloned into the same sites of a modified pET28a(+) vector (p28, removed the thrombin cleave site). The plasmids were cotransformed into *Escherichia coli* BL21(DE3) (Merck) for protein expression. Cells were grown to an OD_{600} of 1.0 at 37 °C and induced with 1 mM IPTG[1] for 20 h at 27 °C.

[†]This work was supported by the Chinese National Natural Science Foundation (Grants 30025012, 30900224, and 10979039), the Chinese Ministry of Science and Technology (Grants 2006CB806500, 2006CB910200, and 2006AA02A318), the Chinese Academy of Sciences (Grant KSCX2-YW-R-60), the Chinese Ministry of Education (Grant 20070358025), and the Natural Science Foundation of Anhui Province (Grant 090413081).

[‡]Atomic coordinates and structure factors for the human NAC domain have been deposited in the Protein Data Bank as entry 3LKX.

*To whom correspondence should be addressed. E-mail: lwniu@ustc.edu.cn or mkteng@ustc.edu.cn. Telephone: 86-551-3606314. Fax: 86-551-3601443.

[1]Abbreviations: IPTG, isopropyl 1-*β*-D-thiogalactoside; Tris, 2-amino-2-(hydroxymethyl)propane-1,3-diol; PEG, polyethylene glycol; DTT, 1,4-dithiothreitol; EDTA, diaminoethanetetraacetic acid; HEPES, 4-(2-hydroxyethyl)-1-piperazineethanesulfonic acid; SDS, sodium dodecyl sulfate; PAGE, polyacrylamide gel electrophoresis; 5′-FAM, 5′-carboxyfluorescein; dsDNA, double-stranded DNA; ssDNA, single-stranded DNA; ssRNA, single-stranded RNA; PBS, phosphate-buffered saline; BSA, bovine serum albumin; DAPI, 4′,6-diamidino-2-phenylindole; PISA, protein interfaces, surfaces, and assemblies service PISA at the European Bioinformatics Institute; rmsd, root-mean-square deviation.

 Published on Web 03/09/2010

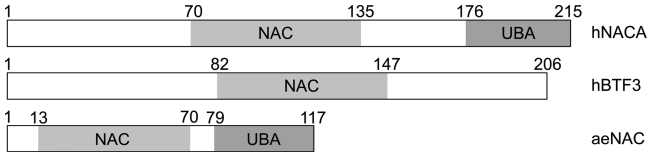

FIGURE 1: Schematic representation of conserved domains in human NAC and the archaebacterial homologue aeNAC from *Mortierella marburgensis*.

Expressed proteins were NACAΔN and BTF3ΔN with a MGHHHHHH tag at the N-terminus. Cells were harvested and disrupted by sonication in 50 mM Tris-HCl (pH 8.0) and 250 mM NaCl. After centrifugation, the supernatant was loaded onto a Ni chelating column (GE Healthcare), and proteins were purified following the protocols. The purified product was mainly a heterodimeric complex of the two truncated subunits, NACAΔN and BTF3ΔN. That was further purified with HiLoad 16/60 Superdex 200 (GE Healthcare). The purified NAC complex was dialyzed in 20 mM Tris-HCl (pH 7.0), 80 mM NaCl, and 5 mM β-mercaptoethanol and concentrated to 20 mg/mL. To obtain the NACAΔN homodimer, we cloned the relevant gene into p28 and expressed and purified the protein by the same process as described above. NACA and BTF3 mutations were introduced using the TaKaRa MutanBEST Kit.

Crystallography. Crystals of the hNAC complex suitable for X-ray diffraction were grown in 15% PEG 6000 and 0.1 M sodium citrate (pH 5.5) using the hanging drop vapor diffusion method at 12 °C for 2 weeks. X-ray diffraction data were collected at 100 K with a cryoprotectant [12% PEG6000, 80 mM sodium citrate (pH 5.5), and 20% glycerol] on beamline 3W1A of the Beijing Synchrotron Radiation Facility at the Institute of High Energy Physics, Chinese Academy of Sciences (detector: marccd). Data were processed using HKL2000 (*24*) and programs in the CCP4 package (*25*).

The crystal structure of the homodimeric NAC domain of the nascent polypeptide-associated complex from *M. marburgensis* [Protein Data Bank (PDB) entry 1TR8] was used as an initial search model for determining the structure of hNAC by the standard molecular replacement method with MOLREP in the CCP4 package (*23*, *26*). The model was further built and refined at 2.5 Å resolution using Refmac5 (*27*) and COOT (*28*) by manual model correction. Cycles of refinement and model building were conducted until the crystallographic *R*-factor and free *R*-factor converged to 21.5 and 25.3%, respectively. The CNS package (*29*) was used during the refinement, and TLS refinement (*30*) was executed in Refmac5 at the last stage. Structure stereochemistry was checked with PROCHECK (*31*). Details about data collection and processing are given in Table 1. Figures were prepared using PyMOL (*32*).

Analysis of NAC−DNA Interactions by an Electrophoretic Mobility Shift Assay. The DNA probe used in the electrophoretic mobility shift assay (EMSA) was synthesized by Sangon with a 5′-CCTTACAGCAAAGCTACTTT-3′ sequence selected at random. Two strands of complementary ssDNA were annealed to form dsDNA. dsDNA (100 nM) was mixed with different amounts of protein and incubated in 20 mM HEPES (pH 7.0), 80 mM NaCl, 1 mM DTT, and 2 mM EDTA at 4 °C for 1 h, before electrophoresis on 8% native-PAGE gels at 60 V in 0.5× TBE buffer at 4 °C. After electrophoresis, the gel was stained with the nucleic acid gel stain GelRed (Biotium, Inc.).

Fluorescence Polarization Assays. The sequences of fluorescently labeled (5′-FAM) DNA and RNA probes were the same as those used in the EMSA (TaKaRa). Fluorescence polarization assays (FPA) were performed in 20 mM HEPES (pH 7.0), 80 mM NaCl, 1 mM DTT, and 2 mM EDTA at 25 °C using a SpectraMax M5 Microplate Reader system. The wavelengths of fluorescence excitation and emission were 490 and 524 nm, respectively. Each 384-well contained 100 nM 5′-FAM-labeled dsDNA probe or 200 nM 5′-FAM-labeled ssDNA or ssRNA probe and different amounts of proteins (concentrations from 0 to 180 μM) in a final volume of 80 μL. For each assay, nucleic acid-free protein-only controls (proteins only) were included. The fluorescence polarization *P* (in mP units) was calculated with eq 1

$$P = \frac{I_{\parallel} - I_{\perp}}{I_{\parallel} + I_{\perp}} \quad (1)$$

The fluorescence polarization change ΔP (in mP units) was fit to eq 2

$$\Delta P = \Delta P_{\max} \frac{[\text{protein}]}{K_d + [\text{protein}]} \quad (2)$$

Immunofluorescence. HeLa cells were cultured in Dulbecco's modified Eagle's medium (DMEM) (Gibco) containing 10% fetal bovine serum (FBS) (Gibco). The P3×FLAG-myc-CMV-24 vector (Sigma) expressing NACA or NACA_Q was transfected into cells using LipofectAMINE 2000 reagent (Invitrogen) at ~60% confluence in Opti-MEM (Gibco). Twenty-four hours after transfection, cells were fixed in 4% paraformaldehyde and permeabilized with 0.1% Triton X-100 in PBS and blocked with 1% BSA in PBS plus 0.05% Tween 20. Cells were incubated with anti-myc antibody (1:300, Santa Cruz) for 1 h at room temperature and washed with PBS plus 0.05% Tween 20 three times,

Table 1: Crystallographic Statistics

Data Collection	
resolution (Å)	50.0−2.50 (2.54−2.50)[a]
wavelength (Å)	1.0000
oscillation width (deg)	1
exposure time (s)	5
space group	$P6_122$
unit cell parameters (Å)	$a = b = 59.76$, $c = 176.82$
no. of unique reflections	7011 (280)[a]
redundancy	17.1 (5.3)[a]
completeness (%)	98.8 (86.4)[a]
average $I/\sigma(I)$	35.8 (1.6)[a]
R_{merge}[b] (%)	6.7 (44.3)[a]
Refinement	
resolution (Å)	50.0−2.50
no. of reflections for refinement/test	6407/529
R_{work}[c] (%)/R_{free}[d] (%)	21.5/25.3
rmsd for bonds (Å)	0.009
rmsd for angles (deg)	1.374
mean *B* factor (Å^2)	25.6
no. of non-hydrogen protein atoms	903
no. of water oxygen atoms	19
Ramachandran plot (%)	
most favored regions	93.1
additional allowed regions	5.9
generously allowed regions	1.0

[a]Values in parentheses are for the highest-resolution shell. [b]$R_{merge} = \sum_h\sum_l|I(h)_l - \langle I(h)\rangle|/\sum_h\sum_l I(h)_l$, where $I(h)_l$ is the *l*th observation of reflection *h* and $\langle I(h)\rangle$ is the weighted average intensity for all observations *l* of reflection *h*. [c]$R_{work} = \sum_h||F_{obs}(h)| - |F_{cal}(h)||/\sum_h|F_{obs}(h)|$, where $F_{obs}(h)$ and $F_{cal}(h)$ are the observed and calculated structure factors for reflection *h*, respectively. [d]R_{free} was calculated as R_{work} using the 8% of reflections that were selected randomly and omitted from refinement.

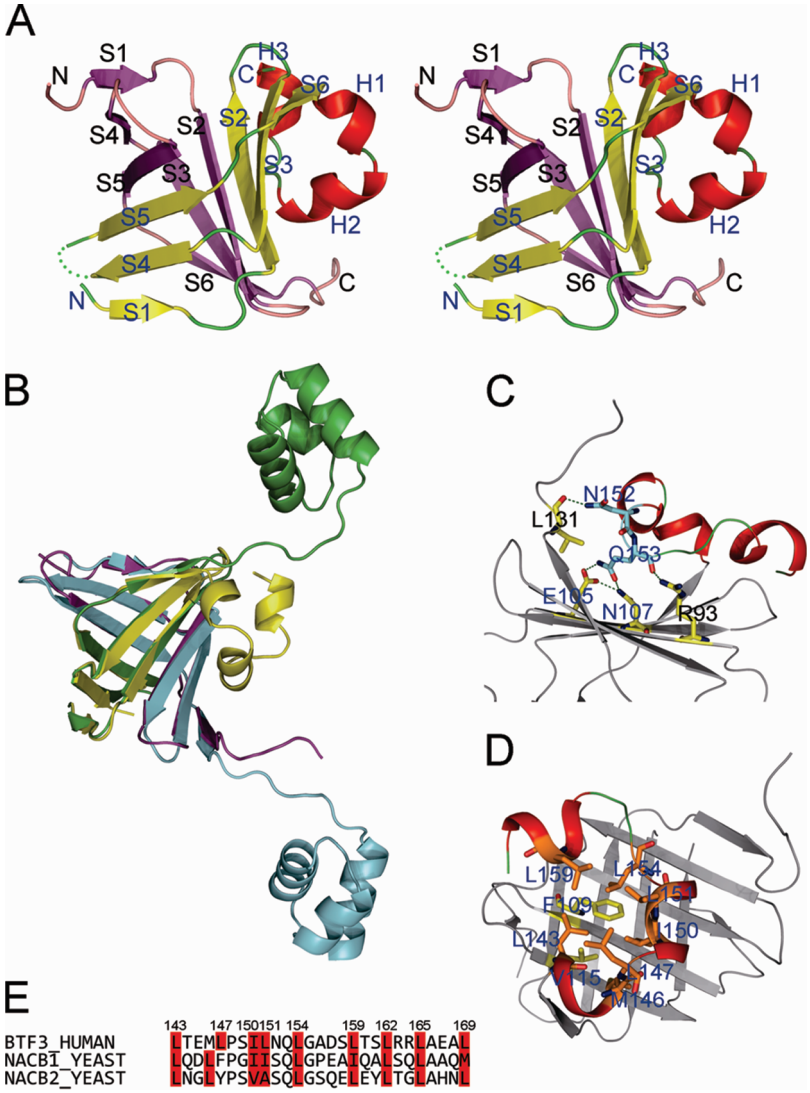

FIGURE 2: Structural features of the human NAC domain. (A) Stereoview of the human NAC domain. NACA is colored purple and BTF3 yellow and red. (B) Overall structure superposition of the hNAC domain with aeNAC. Human NAC is colored yellow and purple and aeNAC green and blue. (C) Residues forming hydrogen bonds between the helix region of BTF3 and the β-sheet region. (D) Residues contributing to hydrophobic interactions between the BTF3 helix region and the β-sheet region. (E) Highlighted leucines and isoleucines in the BTF3 helix region. These residues are conserved between human and yeast β-NAC homologues.

before being incubated for 1 h at room temperature with Texas Red-conjugated anti-mouse IgG secondary antibody (1:300, Santa Cruz) to detect myc-tagged NACA proteins. Digital images were acquired using an IX71 inverted system microscope (Olympus, Tokyo, Japan).

RESULTS

Structure of the Heterodimer of NAC Domains. Human NAC is a heterodimer of NACA and BTF3 subunits. We were unable to obtain full-length complex crystals, so we made truncations of the two subunits based on the structure of an archaebacterial NAC (aeNAC) from *M. marburgensis* (*23*) (Figure S1 of the Supporting Information). NACA with the 83 N-terminal residues truncated (NACAΔN) and BTF3 with the 95 N-terminal residues truncated (BTF3ΔN) still formed a heterodimer, as copurified by Ni affinity chromatography when the six-His tag was linked to the BTF3 subunit, and a sharp elution peak was observed in the gel filtration experiment (Figures S2A and S3 of the Supporting Information). Because of partial degradation during the crystallization process, as proven via SDS−PAGE of dissolved crystals (Figure S2B of the Supporting Information), and the natural disorder of protein in crystal, the final crystal structure exhibited only residues 84−136 of NACA and residues 97−162 of BTF3. This included most of the NAC domains that mediated the heterodimerization, and a short helix region after the NAC domain on the BTF3 subunit (Figure 2A). The two subunits each have six β-strands (S1−S6) and formed a two-side flattened β-barrel with one antiparallel β-sheet on each side. The S1, S4, and S5 strands of the two subunits formed a concave antiparallel β-sheet designed as the "outer" surface, with the S2, S3, and S6 strands forming the "inner" surface. The S2 strands and S5 strands of the two subunits formed intrasubunit antiparallel β-sheets, respectively (Figure S4A of the Supporting Information). A series of highly conserved hydrophobic residues built up the hydrophobic core of the β-barrel (Figure S4B of the Supporting Information).

Structural Comparison with aeNAC. The crystal structure of NAC from *M. marburgensis* (aeNAC) had been determined (*23*). In eukaryotes, NAC is a heterodimer of α- and β-NAC subunits, while aeNAC is a homodimer of one NAC subunit (Figure 1). Both of the two subunits of human NAC (hNAC) are homologous to aeNAC in the NAC domains. In

these domains, the level of sequence identity is 28% between human NACA and aeNAC and 26% between human BTF3 and aeNAC. The structure of the heterodimerized NAC domain of the human nascent chain-associated complex shows a high degree of similarity to that of aeNAC, with the same dimerization pattern. Both of the subunits align well with the NAC domain of aeNAC (Figure 2B). Superimpositions of the hNAC domain with that of aeNAC (residues 26−72) showed a root-mean-square deviation of 1.7 Å over the Cα atoms of NACA (residues 84−130) and 1.4 Å over the Cα atoms of BTF3 (residues 98−142). The high degree of similarity of the two structures indicates the evolutionary conservation of NAC domains.

A main difference between the two complexes is that at the end of the NAC domain (β6), a short loop in aeNAC links the NAC domain and UBA domain, while in hNAC, three helices from BTF3 cover the inner surface of its NAC domain (Figure 2B). This conformation does not appear to result from crystallization but represents the natural state of the protein. Analysis by PISA (*33*) showed that the interface between the helix region and the inner surface was 517 Å^2, and the conformation was predicted to be stable in solution. Several hydrogen bonds formed between the residues of these helices and the NAC domain inner surface; also, a cluster of hydrophobic interactions formed between them. Residues N152 and Q153 of the helix region of BTF3 form hydrogen bonds with R93 and L131 of NACA and with E105 and N107 of BTF3 (Figure 2C). Residues L143, L147, I150, L151, L154, and L159 of the BTF3 helix region form a hydrophobic core with F109 and V115 on the strands of BTF3 (Figure 2D). These interactions between the BTF3 helix region and the inner surface of the complex stabilize the helix region relative to the β-barrel. The leucine and isoleucine in the helix region are highly conserved between yeast and human NAC (Figure 2E), indicating functional conservation. The inner surface of the hNAC domain is buried by the helices and may be blocked from interacting with other proteins or nucleic acids. Instead, the hydrophobic surface of the helices formed by the series of leucines may be involved in interacting with other partners.

Comparison with the NACA Homodimer Model. In the absence of BTF3, NACA alone forms a homodimer and has functions aside from being a polypeptide chaperone, such as regulating transcription (*23*). On the basis of the heterodimer crystal structure, we made a model of the NACA homodimer. Comparing the structure of the hNAC heterodimer with the model of the NACA homodimer, we found that the NACA homodimer inner surface was rich in the positively charged residues arginine and lysine (Figure 3A), while in the hNAC heterodimer, only one lysine was positioned on this surface of BTF3 and the major part of the heterodimer inner surface is masked by the helix region of BTF3 (Figure 3B). The positively charged residues on this surface of the NACA are highly conserved between yeast and human species (Figure 3E). In aeNAC, this surface also has clusters of positively charged residues and was supposed to bind nucleic acids (*23*). The domain architecture of aeNAC and the relatively high level of sequence identity between aeNAC and human NACA suggest that the aeNAC homodimer is more like a human NACA homodimer than a NAC heterodimer. Therefore, the inner surface of the NACA homodimer is also a candidate for binding nucleic acids. On the other side of the β-barrel, a cluster of conserved aromatic (Y112 and F123) and hydrophobic (L85 and I121) residues of the

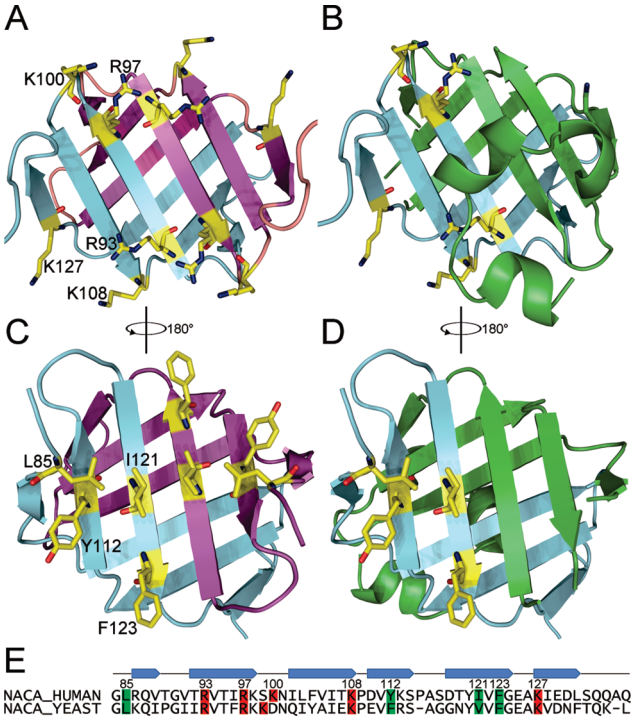

FIGURE 3: Structural comparison of the human NAC domain with the NACA homodimer model. (A) Inner surface of the NACA homodimeric domain model. The positively charged residues on NACA are labeled. (B) Inner surface of the hNAC heterodimeric domain. (C) Outer surface of the NACA homodimeric domain model. The hydrophobic residues on NACA are labeled. (D) Outer surface of the hNAC heterodimeric domain. (E) Highlighted conserved positively charged and hydrophobic residues in the NAC domain of NACA. These residues are conserved between human and yeast α-NAC. Positively charged residues are colored red and hydrophobic residues green.

NACA form a hydrophobic surface (Figure 3D,E). In the NACA homodimer, the number of hydrophobic residues on this outer surface also increases, which may change the function of this surface (Figure 3C). These differences possibly contribute to the different behaviors of NACA in homodimeric and heterodimeric forms.

The Inner Surface of the NACA Homodimer Binds Nucleic Acids. The N-terminally truncated NACAΔN still formed a homodimer (Figures S2C and S3 of the Supporting Information). NACA was previously shown to bind nucleic acids with high affinity (*34*). Its binding to the osteocalcin promoter DNA through residues 69−80 is required for potentiation of c-Jun-dependent transcription of the osteocalcin gene (*17*). To test if the inner surface of the NACA homodimer also bound nucleic acids, we expressed and purified NACAΔN and tested its affinity for DNA. The complex of NACAΔN and BTF3ΔN was used as a control. Since residues 69−80 were excluded from the NACAΔN segment in both the homodimer and the heterodimer, the NACAΔN and BTF3ΔN heterodimer (NACΔN) were not expected to bind DNA, while the NACAΔN homodimer might bind through the patch of exposed positive residues on the inner surface. We tested dsDNA binding via an electrophoretic mobility shift assay (EMSA). As shown in Figure 4A, the NACΔN heterodimer did not cause DNA band shifts, while the NACAΔN homodimer did. This fit with our hypothesis that the NACAΔN homodimer retained DNA binding activity, while in the heterodimer, the NACAΔN DNA-binding surface was covered by the BTF3 subunit.

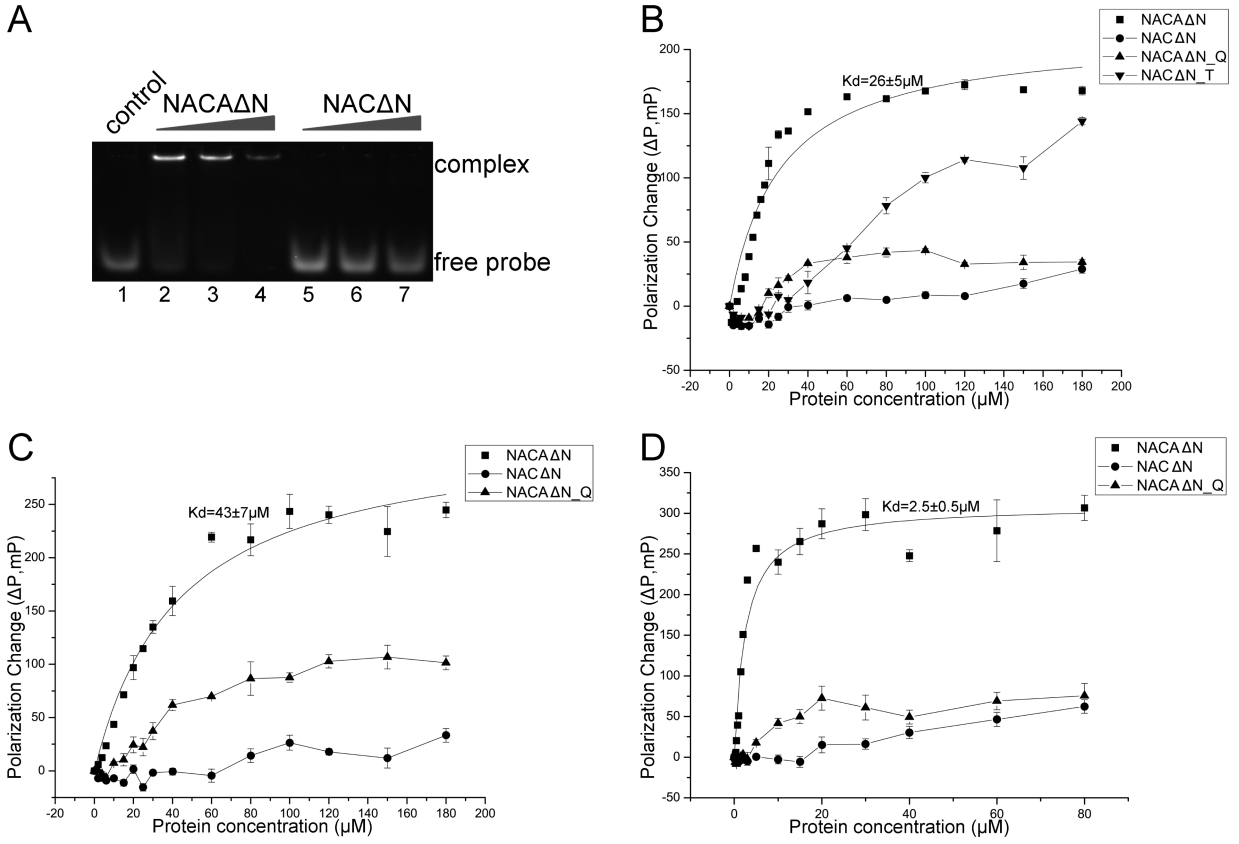

FIGURE 4: Human NACAΔN interacts with nucleic acids through the inner surface. (A) EMSA assessing the interaction of NACAΔN and NACΔN with a random sequence 20 bp dsDNA. Each lane included 10 μM dsDNA. The NACAΔN concentrations were 100, 150, and 200 μM in lanes 2−4, respectively. The NACΔN concentrations were 100, 150, and 200 μM in lanes 5−7, respectively. (B) FPA of NACAΔN, NACΔN, and mutants with 5′-FAM-labeled 20 bp dsDNA. (C) FPA of NACAΔN, NACΔN, and NACAΔN_Q with 5′-FAM-labeled 20 bp ssDNA. (D) FPA of NACAΔN, NACΔN, and NACAΔN_Q with 5′-FAM-labeled 20 bp ssRNA. Data for NACAΔN in each diagram were fitted according to eq 2 (see Materials and Methods). Others did not interact sufficiently strongly for reliable constants.

We then measured the DNA binding abilities of the NACAΔN homodimer and NACΔN by the fluorescence polarization assay (FPA). The dissociation constant (K_d) between the NACAΔN homodimer and dsDNA was approximately 26 μM, and the NACΔN heterodimer caused almost no change in fluorescence polarization (Figure 4B). To test if the positive residues on the inner surface of NACA were responsible for the interaction, we mutated residues R93, R97, K100, and K108 to Q and tested the mutant's affinity for dsDNA. As expected, the affinity of this mutant (NACAΔN_Q) for dsDNA was significantly reduced (Figure 4B). To confirm that the loss of DNA affinity resulted from a block of this surface by the BTF3 helix region in the heterodimer, we made a mutant that truncated the helix region (residue 143−176) from the BTF3ΔN subunit. The new truncated version of BTF3ΔN (BTF3ΔN_T) still formed a heterodimer with NACAΔN (Figures S2A and S3 of the Supporting Information). As measured by FPA, this heterodimer (NACΔN_T) partially recovered the ability to bind dsDNA (Figure 4B). These results indicated that the inner positively charged surface of the NACA homodimer is a novel dsDNA-binding surface that is different from the previously identified DNA-binding region of residues 69−80, and in the NAC heterodimer, this region is blocked by the BTF3 helix region.

We also tested the ability of the NACAΔN homodimer to bind ssDNA using FPA and found that it bound them with a similar but slightly higher K_d (47 μM) (Figure 4C). Similar to the results with dsDNA, NACΔN did not bind ssDNA (Figure 4C). The affinity of NACAΔN_Q for ssDNA was decreased significantly compared to that of NACAΔN, indicating that the inner surface was also responsible for interaction with ssDNA (Figure 4C).

Finally, we tested these proteins' ssRNA binding abilities, which were generally similar to their DNA binding abilities. A striking difference was that NACAΔN bound ssRNA with a much higher affinity than DNA (K_d = 2.5 μM) (Figure 4D). This illustrated that while both DNA and RNA interact with the NACA inner surface, RNA is more likely to be a natural substrate.

The Inner Surface Affects the Subcellular Localization of the NACA Homodimer. HeLa cells were transfected with full-length NACA and NACA_Q mutant expression vectors to determine the effect of the positively charged residues of the inner surface on the subcellular localization of NACA. Wild-type NACA was observed in both the cytosol and nucleus in 61% of the cells, and exclusive cytosolic localization was observed in 39% of the cells (Figure 5). In contrast, in NACA_Q-expressing cells, the percentage of those exhibiting both cytosolic and nuclear sublocalization of the protein decreased to 21%, and in the other 79% of the cells, NACA_Q localized exclusively in the cytosol (Figure 5). Therefore, we concluded that the positively charged inner surface is crucial for NACA localization in the nucleus.

DISCUSSION

NAC is a conserved protein chaperone that shields nascent polypeptides and helps target ribosomes to the endoplasmic reticulum and mitochondria properly. The α- and β-subunits

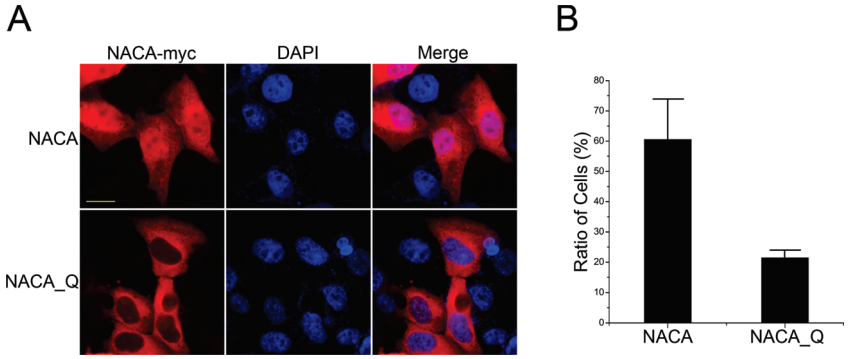

FIGURE 5: Inner surface that affects NACA subcellular localization. (A) HeLa cells were transfected with NACA and NACA_Q expression vectors, and myc-tagged recombinant proteins were detected by indirect immunofluorescence (top row). Nuclei were stained with DAPI (bottom row). The bar is 10 μm. (B) Statistics of the ratios of cells in which NACA or NACA_Q was localized both in the cytosol and in the nucleus.

of NAC form a heterodimer to perform this function. In this study, we determined the crystal structure of the dimerization domain of the human NAC. This is the first report to use the crystal structure to determine the manner of heterodimerization of eukaryotic NAC. The structure suggests that from archaea to humans, NAC changes from a homodimer to a heterodimer, but the mechanism of dimerization of NAC domains is highly conserved, with binding by two pairs of β-sheets to form a β-barrel. Six β-strands from each subunit are the minimal components for the formation of an NAC complex.

Besides the function as a protein chaperone, the NACA subunit has a high affinity for nucleic acids and is a coactivator in transcription regulation (*17*, *34*). It binds the osteocalcin promoter DNA through residues 69−80 (*17*). We identified the inner surface of the NAC domain as another nucleic acid-binding region of the NACA homodimer. This region may function in several possible ways. First, since residues 69−80 are just N-terminal to the NAC domain of NACA, the two DNA-binding regions are spatially close. Therefore, this region may also be required for transcription coactivator function. The inner surface may assist in NACA's correct location of the specific promoter regions and in strengthening the interaction between NACA and the promoter DNA. Our results showed that NACA bound RNA through the inner surface of the NAC domain with much higher affinity than DNA. This suggests the possibility that NACA functions in post-transcriptional processes such as assisting in RNA stability and translocation.

While the NAC heterodimer is located mainly in the cytosol, NACA is distributed to both the cytosol and the nucleus (*14*, *34*). The transport of NACA from the cytosol to the nucleus is prompted by phosphorylation of serine 43 (*35*, *36*). In our experiments, after the nucleic acid-binding residues on the NACA inner surface had been mutated, the degree of localization of NACA in the nucleus diminished remarkably. This indicates that the nucleic acid-binding inner surface is also important for assuring the correct distribution and function in the nucleus. The transcription coactivator activity of NACA is inhibited by the existence of BTF3 (*14*). Also, in certain types of cells, NACA is far more abundant than BTF3 (*14*). Combined with our results, a model for regulation of NACA subcellular distribution and function through regulation of the proportion of NACA relative to BTF3 has emerged. When the two proteins are expressed in stoichiometric amounts, NACA remains in the cytosol to form a heterodimer with BTF3 and functions as a molecular chaperone in post-translational processes. Under certain conditions, NACA is expressed at higher levels than BTF3, causing it to form a homodimer and to enter the nucleus to function in the transcription-related processes. The exposed inner surface assists NACA's localization and/or functions in the nucleus by binding nucleic acids. BTF3 blocks the inner surface of NACA from binding nucleic acids, providing a regulatory mechanism for NACA homo- and heterodimer functions.

The cell is an economic system, and its components are usually employed with high efficiency. Therefore, it is common for one protein to carry multiple functions. The switching of NACA between protein chaperone and transcription coactivator functions through the formation of hetero- or homodimers provides a link between translation and transcription. The exact mechanisms of NAC and NACA functions are still unknown, and the biochemical difference between the NAC heterodimer and NACA homodimer is still not fully understood. The NAC domain may serve only as a module for forming dimers, or it may have other functions. The crystal structure of the human NAC domain shows new features in the subunit conformations, and the newly identified nucleic acid-binding region of NACA provides possible explanations about the regulation of its function. These results also provide more details about the biological function of NAC.

ACKNOWLEDGMENT

We thank Dr. Yuhui Dong and Dr. Zengqiang Gao for assistance with data collection at beamline 3W1A of the Beijing Synchrotron Radiation Facility at the Institute of High Energy Physics, Chinese Academy of Sciences. We thank Dr. Dongmei Wang and Dr. Zheng Ying for assistance and advice in cell culturing and the immunofluorescence assay. We thank Dr. Jianye Zang for helpful advice on experiments and the manuscript.

SUPPORTING INFORMATION AVAILABLE

Figure S1 shows the sequeuce alignments between human NAC subunits and aeNAC. Figure S2 summarized the SDS-PAGE analysis results of proteins used for crystal and biochemical analyses. Figure S3 shows the results of analyses of the proteins' homogeneities by Gel Exclusion Chromatography. Figure S4 shows the residues forming intersubunit β-sheets and hydrophobic core of hNAC heterodimer. This material is available free of charge via the Internet at http://pubs.acs.org.

REFERENCES

1. Agashe, V. R., and Hartl, F. U. (2000) Roles of molecular chaperones in cytoplasmic protein folding. *Semin. Cell Dev. Biol. 11*, 15–25.

2. Kramer, G., Boehringer, D., Ban, N., and Bukau, B. (2009) The ribosome as a platform for co-translational processing, folding and targeting of newly synthesized proteins. *Nat. Struct. Mol. Biol. 16*, 589–597.
3. Wiedmann, B., Sakai, H., Davis, T. A., and Wiedmann, M. (1994) A protein complex required for signal-sequence-specific sorting and translocation. *Nature 370*, 434–440.
4. Wegrzyn, R. D., Hofmann, D., Merz, F., Nikolay, R., Rauch, T., Graf, C., and Deuerling, E. (2006) A conserved motif is prerequisite for the interaction of NAC with ribosomal protein L23 and nascent chains. *J. Biol. Chem. 281*, 2847–2857.
5. Lauring, B., Wang, S., Sakai, H., Davis, T. A., Wiedmann, B., Kreibich, G., and Wiedmann, M. (1995) Nascent-polypeptide-associated complex: A bridge between ribosome and cytosol. *Cold Spring Harbor Symp. Quant. Biol. 60*, 47–56.
6. Wang, S., Sakai, H., and Wiedmann, M. (1995) NAC covers ribosome-associated nascent chains thereby forming a protective environment for regions of nascent chains just emerging from the peptidyl transferase center. *J. Cell Biol. 130*, 519–528.
7. Lauring, B., Sakai, H., Kreibich, G., and Wiedmann, M. (1995) Nascent polypeptide-associated complex protein prevents mistargeting of nascent chains to the endoplasmic reticulum. *Proc. Natl. Acad. Sci. U.S.A. 92*, 5411–5415.
8. Funfschilling, U., and Rospert, S. (1999) Nascent polypeptide-associated complex stimulates protein import into yeast mitochondria. *Mol. Biol. Cell 10*, 3289–3299.
9. Lauring, B., Kreibich, G., and Weidmann, M. (1995) The intrinsic ability of ribosomes to bind to endoplasmic reticulum membranes is regulated by signal recognition particle and nascent-polypeptide-associated complex. *Proc. Natl. Acad. Sci. U.S.A. 92*, 9435–9439.
10. George, R., Beddoe, T., Landl, K., and Lithgow, T. (1998) The yeast nascent polypeptide-associated complex initiates protein targeting to mitochondria in vivo. *Proc. Natl. Acad. Sci. U.S.A. 95*, 2296–2301.
11. Panasenko, O., Landrieux, E., Feuermann, M., Finka, A., Paquet, N., and Collart, M. A. (2006) The yeast Ccr4-Not complex controls ubiquitination of the nascent-associated polypeptide (NAC-EGD) complex. *J. Biol. Chem. 281*, 31389–31398.
12. Panasenko, O. O., David, F. P., and Collart, M. A. (2009) Ribosome association and stability of the nascent polypeptide-associated complex is dependent upon its own ubiquitination. *Genetics 181*, 447–460.
13. Hiraishi, H., Shimada, T., Ohtsu, I., Sato, T. A., and Takagi, H. (2009) The yeast ubiquitin ligase Rsp5 downregulates the α subunit of nascent polypeptide-associated complex Egd2 under stress conditions. *FEBS J. 276*, 5287–5297.
14. Yotov, W. V., Moreau, A., and St-Arnaud, R. (1998) The α chain of the nascent polypeptide-associated complex functions as a transcriptional coactivator. *Mol. Cell. Biol. 18*, 1303–1311.
15. Moreau, A., Yotov, W. V., Glorieux, F. H., and St-Arnaud, R. (1998) Bone-specific expression of the α chain of the nascent polypeptide-associated complex, a coactivator potentiating c-Jun-mediated transcription. *Mol. Cell. Biol. 18*, 1312–1321.
16. Quelo, I., Hurtubise, M., and St-Arnaud, R. (2002) αNAC requires an interaction with c-Jun to exert its transcriptional coactivation. *Gene Expression 10*, 255–262.
17. Akhouayri, O., Quelo, I., and St-Arnaud, R. (2005) Sequence-specific DNA binding by the αNAC coactivator is required for potentiation of c-Jun-dependent transcription of the osteocalcin gene. *Mol. Cell. Biol. 25*, 3452–3460.
18. Rospert, S., Dubaquie, Y., and Gautschi, M. (2002) Nascent-polypeptide-associated complex. *Cell. Mol. Life Sci. 59*, 1632–1639.
19. Lopez, S., Stuhl, L., Fichelson, S., Dubart-Kupperschmitt, A., St Arnaud, R., Galindo, J. R., Murati, A., Berda, N., Dubreuil, P., and Gomez, S. (2005) NACA is a positive regulator of human erythroid-cell differentiation. *J. Cell Sci. 118*, 1595–1605.
20. Hu, G. Z., and Ronne, H. (1994) Yeast BTF3 protein is encoded by duplicated genes and inhibits the expression of some genes in vivo. *Nucleic Acids Res. 22*, 2740–2743.
21. Zheng, X. M., Black, D., Chambon, P., and Egly, J. M. (1990) Sequencing and expression of complementary DNA for the general transcription factor BTF3. *Nature 344*, 556–559.
22. Meury, T., Akhouayri, O., Jafarov, T., Mandic, V., and St-Arnaud, R. (2010) Nuclear αNAC influences bone matrix mineralization and osteoblast maturation in vivo. *Mol. Cell. Biol. 30*, 43–53.
23. Spreter, T., Pech, M., and Beatrix, B. (2005) The crystal structure of archaeal nascent polypeptide-associated complex (NAC) reveals a unique fold and the presence of a ubiquitin-associated domain. *J. Biol. Chem. 280*, 15849–15854.
24. Otwinowski, Z., and Minor, W. (1997) Processing of X-ray diffraction data collected in oscillation mode. *Methods Enzymol. 276*, 307–326.
25. Collaborative Computational Project Number 4 (1994) The CCP4 suite: Programs for protein crystallography. *Acta Crystallogr. D50*, 760–763.
26. Vagin, A., and Teplyakov, A. (2000) An approach to multi-copy search in molecular replacement. *Acta Crystallogr. D56*, 1622–1624.
27. Murshudov, G. N., Vagin, A. A., and Dodson, E. J. (1997) Refinement of macromolecular structures by the maximum-likelihood method. *Acta Crystallogr. D53*, 240–255.
28. Emsley, P., and Cowtan, K. (2004) Coot: Model-building tools for molecular graphics. *Acta Crystallogr. D60*, 2126–2132.
29. Brunger, A. T., Adams, P. D., Clore, G. M., DeLano, W. L., Gros, P., Grosse-Kunstleve, R. W., Jiang, J. S., Kuszewski, J., Nilges, M., Pannu, N. S., Read, R. J., Rice, L. M., Simonson, T., and Warren, G. L. (1998) Crystallography & NMR system: A new software suite for macromolecular structure determination. *Acta Crystallogr. D54*, 905–921.
30. Winn, M. D., Murshudov, G. N., and Papiz, M. Z. (2003) Macromolecular TLS refinement in REFMAC at moderate resolutions. *Methods Enzymol. 374*, 300–321.
31. Laskowski, R. A., MacArthur, M. W., Moss, D. S., and Thornton, J. M. (1993) PROCHECK: A program to check the stereochemical quality of protein structures. *J. Appl. Crystallogr. 26*, 283–291.
32. DeLano, W. L. (2002) The PyMOL Molecular Graphics System, DeLano Scientific, San Carlos, CA.
33. Krissinel, E., and Henrick, K. (2007) Inference of macromolecular assemblies from crystalline state. *J. Mol. Biol. 372*, 774–797.
34. Beatrix, B., Sakai, H., and Wiedmann, M. (2000) The α and β subunits of the nascent polypeptide-associated complex have distinct functions. *J. Biol. Chem. 275*, 37838–37845.
35. Quelo, I., Gauthier, C., Hannigan, G. E., Dedhar, S., and St-Arnaud, R. (2004) Integrin-linked kinase regulates the nuclear entry of the c-Jun coactivator α-NAC and its coactivation potency. *J. Biol. Chem. 279*, 43893–43899.
36. Quelo, I., Akhouayri, O., Prud'homme, J., and St-Arnaud, R. (2004) GSK3β-dependent phosphorylation of the αNAC coactivator regulates its nuclear translocation and proteasome-mediated degradation. *Biochemistry 43*, 2906–2914.